JOURNAL OF COMPUTATIONAL PHYSICS 27, 42–70 (1978)

Steady Flow of a Non-Newtonian Fluid through a Contraction

THOMAS B. GATSKI*

Department of Aerospace Engineering, The Pennsylvania State University, University Park, Pennsylvania 16802

AND

JOHN L. LUMLEY

Sibley School of Mechanical and Aerospace Engineering, Cornell University, Ithaca, New York 14853

Received November 15, 1976; revised June 6, 1977

The equations describing the steady two-dimensional flow of a dilute suspension of macromolecules, a non-Newtonian fluid, are numerically modeled using a finite-difference technique. The flow domain is composed of a parallel-walled inflow region, a contraction region in which the walls are rectangular hyperbolas and a parallel-walled outflow region. The problem is formulated in terms of the vorticity and stream function along with explicit dependence on the deviatoric stresses. For a Newtonian fluid the relationship between stress and deformation rate is a linear one; however, for a non-Newtonian fluid the relationship is more complex. Here the constitutive equation used is a three constant Oldroyd equation which is valid for dilute polymer solutions. Due to a singularity in the transformation to a natural set of coordinates (with respect to the contraction boundary) a Cartesian grid system is used throughout the domain. The irregular grid structure at the curved boundaries necessitates developing a method for determining the boundary values of the vorticity, stream function and stresses. An explicit differencing scheme is used to model the governing equations, with the advection terms in the equations modeled using upstream differencing. The effect of numerical viscosity on the flow structure is examined with respect to the boundary layer thickness along the curved boundary and, in addition, contour plots of the flow variables are presented for both the non-Newtonian fluid and the Newtonian solvent fluid.

1. INTRODUCTION

The equations governing the flow in the two-dimensional flow domain are found from first principles and an appropriate rheological equation of state. Figure 1 shows the flow domain with the contraction boundary given by $xy = 0.08$. As is seen from the figure, the domain is divided into three regions: a 1-in. inflow region, a 1-in. contraction region, and a 0.5-in. outflow region. The inflow and outflow regions allow for uniform entrance and exit conditions to be specified and, due to the symmetry of

* Permanent Address: NASA Langley Research Center, Hampton, Va. 23665.

0021-9991/78/0271-0042$02.00/0

the domain, one need only solve for the flow in half of the field. Such a contraction region is of interest since along the centerline the flow is irrotational and solenoidal, hence a pure straining motion. This type of extensional flow can be of interest in examining molecular elongation and variations of intrinsic viscosity with longitudinal gradient [1]. For water and most gases the equation of state is found to be simply a linear relationship between stress and deformation rate over a wide range of values of the latter; however, for dilute polymer solutions, the equation of state, or constitutive equation, is more complex. Giesekus [2] (or [3]) has shown that dilute solutions of

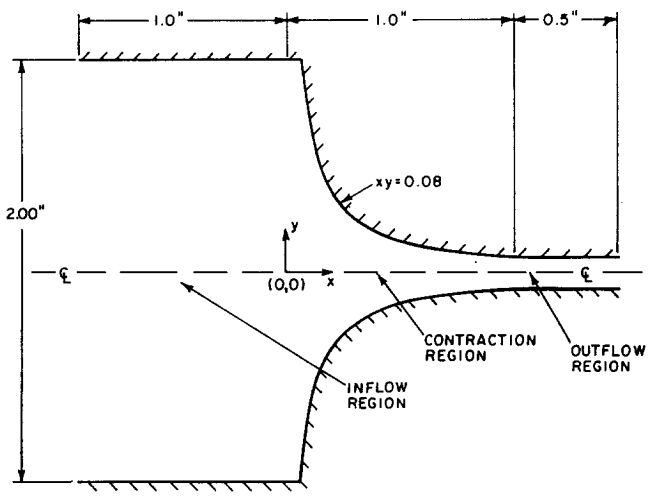

FIG. 1. Flow domain.

polymers obey the Oldroyd equation [4] to first approximation. Unfortunately, the Oldroyd constitutive equations coupled with the appropriate conservation equations form a system of equations which are intractable analytically in this two-dimensional contracting flow.

It is necessary then to resort to numerical techniques to solve the governing system of equations; in particular, the finite-difference technique is used in this investigation. Gatski [5] has applied the finite-difference method to a time dependent one-dimensional Oldroyd model equation (valid along the centerline of this contraction) which included advection terms which were missing in previous numerical work, such as that by Townsend [6], who employed a finite-difference technique on an Oldroyd equation for rectilinear flow in a straight pipe of circular cross section. Gatski [5] found that the time increment restriction was rather severe for the proposed explicit scheme, thus requiring alternatives such as an implicit scheme or a steady-state analysis. Since the purpose here is to set forth a method for examining the basic flow structure of the non-Newtonian fluid in the domain, a steady-state analysis is quite sufficient. The only feature of the transient problem is the oscillatory behavior of the flow variables [5, 6].

A Cartesian grid system is used throughout the entire flow domain, including the contraction region (due to a singularity in the transformation to a more natural set of coordinates), thus creating an irregular grid cell structure adjacent to the curved boundary. At node points adjacent to the curved boundary symmetry conditions are derived for the different flow variables in order to solve the governing difference equations. Finally, the equations for the non-Newtonian fluid exhibit elastic propagation effects [7], making it desirable to preserve the transportive property in the difference equations. In order to do this, upstream differencing of the advection terms is used. This type of differencing causes artificial viscosity errors, the extent of which is analyzed in Section 5, but still allows adequate representation of the flow field at values of the ratio of molecular relaxation time to flow time scale less than one.

2. The Motion and Non-Newtonian Constitutive Equations

In describing the flow of a dilute polymer solution (the non-Newtonian fluid), appropriate motion and constitutive equations are needed. Since in this investigation the fluid is incompressible (the motion then being isochoric and the velocity vector solenoidal) and there are no external body forces, the governing motion and constitutive equations [2, 3] for the flow of the dilute polymer solutions are

$$\dot{u}_i + u^j u_{i,j} = -P_{,i} + g_{ik}\tau^{kj}, \tag{2.1}$$

$$\tau^{kj} + \lambda_1 \frac{\delta\tau^{kj}}{\delta t} = \frac{2(1 + c[\eta])}{R_s} S^{kj} + \frac{2\lambda_1}{R_s}\frac{\delta S^{kj}}{\delta t}, \tag{2.2}$$

where

$$\frac{\delta\tau^{kj}}{\delta t} = \dot{\tau}^{kj} + u^m\tau^{kj}_{,m} - u^k_{,m}\tau^{mj} - u^j_{,m}\tau^{km}, \tag{2.3}$$

$$S^{kj} = \tfrac{1}{2}(u^{k,j} + u^{j,k}), \tag{2.4}$$

P is the pressure ($P = -\frac{1}{3} \times$ trace of total stress tensor), u_i and u^j covariant and contravariant velocity vectors, respectively, $R_s = UL/\nu$ is the solvent Reynolds number based on the mean inflow velocity U and the half-width of the inflow region, L, ν is the kinematic viscosity of the solvent (water) ($= 10^{-2}$ cm^2/sec), S^{kj} is the contravariant strain rate tensor, λ_1 is the molecular relaxation time (dimensionless), c is the concentration, $[\eta]$ is the intrinsic viscosity and g_{ij} is the metric tensor. In general, throughout, subscripts and superscripts preceded by a comma indicate covariant and contravariant spatial differentiation, respectively, and a dot over a variable indicates partial differentiation with respect to time. Equation (2.3) can be recognized as the Oldroyd convective derivative [4] and the constitutive equation, Eq. (2.2), corresponds to the Oldroyd B fluid (the B fluid exhibits the positive Weissenberg effect, climbing up the inner cylinder of a coaxial cylinder device) [4]. The Oldroyd B fluid does not exhibit any shear thinning behavior, that is, change of

apparent viscosity with shear. Note that in the limit of zero relaxation time and molecular concentration the constitutive equation reduces to the usual Newtonian linear relationship between stress and deformation rate. Since the flow field under consideration is two-dimensional, the problem lends itself to a vorticity-stream function formulation.

For an orthogonal coordinate system it can be shown that a scalar function of position and time, the stream function, identically satisfies the condition of a solenoidal velocity field ($u^i_{,i} = 0$) if

$$u^1 = (g_{11}g_{22})^{-1/2}\,\psi_{,2}\,, \tag{2.5}$$

$$u^2 = -(g_{11}g_{22})^{-1/2}\,\psi_{,1}\,. \tag{2.6}$$

Now the vorticity is defined as the curl of the velocity and is given by

$$\omega^l = \epsilon^{lni} u_{i,n}\,, \tag{2.7}$$

where ϵ^{lni} is a tensor density, or permutation symbol, and ω^l is a pseudovector. The vorticity equation can be simply derived by taking the curl of Eq. (2.1), which, after some simplification, gives

$$\dot{\omega}^l + u^j\omega^l_{,j} = \epsilon^{lni}\tau^j_{i,jn}\,. \tag{2.8}$$

Up to this point the equations have been derived in a completely general fashion. The generality was needed since at the curved boundary it will be necessary to know the vorticity, stresses, and deformation rates in an orthogonal curvilinear system which is parallel and perpendicular at the same boundary. For the interior of the flow domain, however, a Cartesian grid system is appropriate and the preceding equations can be greatly simplified.

In a Cartesian system, for this flow, the velocity can be expressed as

$$u_i = (u(x, y), v(x, y), 0), \tag{2.9}$$

where the x and y directions for the flow field are as shown in Fig. 1 and the flow field is assumed steady. Now Eqs. (2.5) and (2.6) become

$$u = \psi_y\,, \tag{2.10}$$

$$v = -\psi_x\,, \tag{2.11}$$

where the subscripts x and y indicate partial differentiation with respect to that coordinate direction. The vorticity can now be expressed in the familiar form

$$\omega = v_x - u_y = -\nabla^2\psi, \tag{2.12}$$

where the superscript on ω has been omitted since the only vorticity component is the

one perpendicular to the x–y plane. Since the flow is assumed steady, the vorticity equation, Eq. (2.8), can be written as

$$u\omega_x + v\omega_y = \frac{\partial(\psi, \omega)}{\partial(x, y)} = \tau^{12}_{xx} - \tau^{12}_{yy} + (\tau^{22} - \tau^{11})_{xy} . \tag{2.13}$$

Finally, the stress equation, Eq. (2.2), can be expanded to give

$$\tau^{12} + \lambda_1[u\tau^{12}_x + v\tau^{12}_y - \tau^{22}u_y - \tau^{11}v_x]$$
$$= \frac{2(1 + c[\eta])}{R_s} S^{12} + \frac{2\lambda_1}{R_s}[uS^{12}_x + vS^{12}_y - S^{22}u_y - S^{11}v_x], \tag{2.14}$$

$$\tau^{11} + \lambda_1[u\tau^{11}_x + v\tau^{11}_y - 2\tau^{12}u_y - 2u_x\tau^{11}]$$
$$= \frac{2(1 + c[\eta])}{R_s} S^{11} + \frac{2\lambda_1}{R_s}[uS^{11}_x + vS^{11}_y - 2S^{12}u_y - 2S^{11}u_x], \tag{2.15}$$

$$\tau^{22} + \lambda_1[u\tau^{22}_x + v\tau^{22}_y - 2\tau^{12}v_x - 2\tau^{22}v_y]$$
$$= \frac{2(1 + c[\eta])}{R_s} S^{22} + \frac{2\lambda_1}{R_s}[uS^{22}_x + vS^{22}_y - 2S^{12}v_x - 2S^{22}v_y], \tag{2.16}$$

where

$$S^{12} = \tfrac{1}{2}(u_y + v_x) = \tfrac{1}{2}(\psi_{yy} - \psi_{xx}), \tag{2.17}$$

$$S^{11} = -S^{22} = u_x = -v_y = \psi_{xy} . \tag{2.18}$$

All that is needed now to form a well-posed problem is the specification of the boundary conditions.

3. Boundary Conditions

In Equation (2.12) it is necessary to specify either the value of ψ (Dirichlet condition) or its normal derivative (Neumann condition) along the boundaries of the flow domain. Here we will do the Dirichlet problem and begin by specifying the values of the stream function at the entrance to the flow domain. These values are easily found by integrating the inflow velocity profile. Assuming that at the entrance to the inflow region the velocity profile is parabolic, the distribution of stream function values at the entrance to the domain can be written as

$$\psi(x, y) = (y/2)(3 - y^2), \qquad x < -1, \tag{3.1}$$

where -1 is the nondimensional streamwise location of the entrance to the inflow region (see Figs. 1 and 2). Here the stream function value at $y = 0$, the centerline, has been taken equal to zero. Along the solid wall the value of the stream function must also be constant and from Eq. (3.1), evaluated at $y = 1.0$, is equal to unity. The

condition at the exit of the outflow region is difficult to specify accurately. In this investigation the straight outflow section was assumed to be sufficiently long that the u velocity was simply a function of y. Computational experiments indicated that this assumption was quite satisfactory and no adverse behavior at the exit resulted. In summary, the conditions on ψ along the boundary of the flow domain are

$$\psi = 0.0 \qquad \text{along centerline,} \tag{3.2}$$

$$\psi = (y/2)(3 - y^2) \qquad \text{at entrance,} \tag{3.3}$$

$$\psi = 1.0 \qquad \text{along solid boundary,} \tag{3.4}$$

and

$$\psi(x, y) = \psi(y), \qquad x > 1.5, \tag{3.5}$$

where 1.5 is the nondimensional streamwise location of the exit to the outflow region (see Figs. 1 and 2).

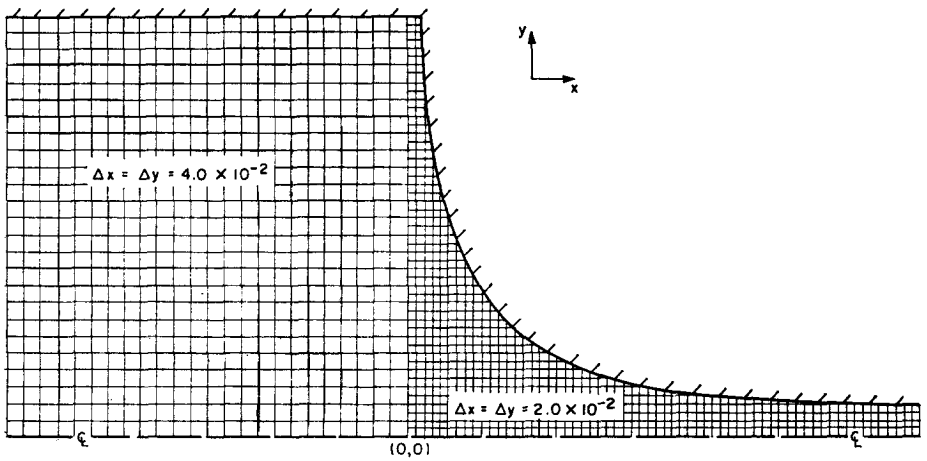

FIG. 2. Cartesian grid system.

Now consider the vorticity equation. In the Newtonian limit the right-hand side of Eq. (2.13) would be proportional to the Laplacian of vorticity and, once again, either the function or its normal derivative must be specified along the boundary of the flow domain. From this one can infer that for the non-Newtonian problem both the vorticity and stresses need to be specified along the boundaries of the domain. Let us first determine the vorticity conditions.

Along the centerline ($y = 0$) and at the entrance the vorticity is determined by differentiating Eq. (3.1). Along the parallel-walled section of the solid boundary and at the exit of the domain the vorticity is given by Eq. (2.12), subject to the conditions of nonporous solid walls and a nonevolving flow in the streamwise direction, respec-

tively. Finally, the specification of the boundary condition along the curved section of the boundary requires additional analysis.

The above statements about vorticity hold true for the curved boundary but with respect to a coordinate system which is parallel and perpendicular to the boundary. So it is first necessary to specify the above conditions in this orthogonal curvilinear system and then transform them back to the Cartesian system (see Appendix A for the construction of the coordinate system). In order to specify the vorticity along the boundary, the expressions for the velocities in the curvilinear system must be known. Using Eqs. (2.5), (2.6), and (A16), one obtains for the physical components of the velocity vector

$$u(\phi) = \{4(\phi^2 + \eta^2)\}^{1/4}\, \psi_\eta\,, \tag{3.6}$$

$$u(\eta) = -\{4(\phi^2 + \eta^2)\}^{1/4}\, \psi_\phi\,, \tag{3.7}$$

where the subscripts ϕ and η indicate partial differentiation with respect to that coordinate. From Equations (2.7), (3.6), and (3.7) the vorticity can be written in the curvilinear system as

$$\omega = J^{-1}\{(g_{22}^{1/2}u(\eta))_\phi - (g_{11}^{1/2}u(\phi))_\eta\} = -2(\phi^2 + \eta^2)^{1/2}(\psi_{\phi\phi} + \psi_{\eta\eta}), \tag{3.8}$$

where J is the Jacobian of the transformation and is equal to $(g_{11}g_{22})^{1/2}$. Since ω is everywhere perpendicular to both the x–y and ϕ–η planes, Eq. (3.8) can be used to determine the vorticity boundary conditions along the curved wall (subject to the condition of zero tangential and normal velocities and $\psi_{\phi\phi} = 0$). In summary the vorticity boundary conditions are

$\omega = 0$	along centerline,	(3.9)
$\omega = -3y$	at entrance,	(3.10)
$\omega = -\psi_{yy}$	along solid boundary (straight section),	(3.11)
$\omega = -2[\phi^2 + (0.08)^2]\, \psi_{\eta\eta}$	along solid boundary (curved section),	(3.12)
$\omega = -\psi_{yy}$	at exit.	(3.13)

Next let us examine the stress conditions.

Since the flow is symmetric about the centerline, the τ^{12} shear stress equation, Eq. (2.14), can be written here as

$$\tau^{(m)12} + u\lambda_1\tau_x^{(m)12} = 0, \tag{3.14}$$

where $\tau^{(m)12}$ ($\equiv \tau^{12} - 2R_s^{-1}S^{12}$) is the extra stress due to the presence of the molecules and along the centerline is equal to τ^{12} due to the fact that the Newtonian stress is zero there. From the solution of Eq. (3.14) one can see, that if the molecules are unstretched at the entrance to the flow domain, the τ^{12} shear stress boundary condition along the centerline of the flow is zero. A cursory treatment of the normal stress equations, Eqs. (2.15) and (2.16), quickly reveals that these equations are rather

cumbersome to handle as boundary conditions along the centerline, even with the use of flow symmetry conditions. As will be seen in the next section, however, the differencing scheme used on these equations makes it unnecessary to use these conditions.

At the entrance to the flow domain the flow is assumed parallel: therefore, the stress conditions applicable at the entrance are

$$\tau^{12} = 2(1 + c[\eta])(1/R_s)\, S^{12}, \tag{3.15}$$

$$\tau^{11} = (8/R_s)\, \lambda_1 c[\eta](S^{12})^2, \tag{3.16}$$

$$\tau^{22} = 0.0. \tag{3.17}$$

Note that the above conditions on the shear and normal stresses hold for any parallel flow. Let us now consider the boundary conditions on the solid walls. Using the conditions that the tangential and normal velocities are zero along the parallel solid boundaries, one can obtain from Eqs. (2.14) through (2.16) the boundary conditions on the stresses there. The shear and normal stress conditions that result are given by Eqs. (3.15) through (3.17), thus indicating that the stress distribution on the solid walls (straight) behaves as though the stress distribution were along the centerline of a parallel flow. In order to determine the conditions on the stresses for the curved boundary it is necessary to formulate Eqs. (2.14) through (2.16) in terms of the ϕ–η coordinates and use the conditions of zero normal and tangential velocity. The resulting conditions on the physical components of the shear and normal stresses along the curved boundary ($\eta = 0.08$) are

$$\tau(\phi, \eta) = 2(1 + c[\eta])(1/R_s)\, S(\phi, \eta), \tag{3.18}$$

$$\tau(\phi, \phi) = (8/R_s)\, \lambda_1 c[\eta](S(\phi, \eta))^2, \tag{3.19}$$

$$\tau(\eta, \eta) = 0.0, \tag{3.20}$$

where along the boundary

$$S(\phi, \eta) = (\phi^2 + (0.08)^2)^{1/2}\, \psi_{\eta\eta}\,. \tag{3.21}$$

However, unlike vorticity, which is the same in both coordinate systems, these stress values must be converted to the Cartesian system. The transformation law for the physical component of a second-order tensor from the curvilinear system to the Cartesian system can be written as

$$\tau^{ij} = X_k{}^j X_i{}^l \tau(l, k), \tag{3.22}$$

where

$$X_k{}^j = \partial \hat{x}^j / \partial x^k, \tag{3.23}$$

$$X_i{}^l = \partial x^l / \partial \hat{x}^i. \tag{3.24}$$

Here the $\hat{x}^j$ coordinates are Cartesian coordinates and the x^l are (ϕ, η) coordinates.

Using these transformation equations and the expressions for the shear and normal stresses in the curvilinear system, one can obtain the Cartesian components of these stresses along the curved boundary,

$$\tau^{12} = 2\phi(1 + c[\eta])(1/R_s)\,\psi_{\eta\eta} - 0.32(\phi^2 + (0.08)^2)^{1/2}\,\lambda_1 c[\eta](1/R_s)(\psi_{\eta\eta})^2, \tag{3.25}$$

$$\tau^{11} = 0.16(1 + c[\eta])(1/R_s)\,\psi_{\eta\eta} + 4(\phi^2 + (0.08)^2)^{1/2} \times (\phi + (\phi^2 + (0.08)^2)^{1/2})\,\lambda_1(1/R_s)\,c[\eta](\psi_{\eta\eta})^2, \tag{3.26}$$

$$\tau^{22} = -0.16(1 + c[\eta])(1/R_s)\,\psi_{\eta\eta} + 4(\phi^2 + (0.08)^2)^{1/2} \times (-\phi + (\phi^2 + (0.08)^2)^{1/2})\,\lambda_1(1/R_s)\,c[\eta](\psi_{\eta\eta})^2. \tag{3.27}$$

Now that the stress conditions along the solid walls have been specified all that remains in the specification of the boundary conditions is to determine the stress behavior at the exit of the domain. These conditions can be easily determined if one recalls that at the exit of the domain the flow was assumed parallel; hence the same assumption here allows us to use the stress conditions, Eqs. (3.15) through (3.17), for the exit boundary conditions. Finally, for completeness, the boundary conditions on the strain rates, Eqs. (2.17) and (2.18), are obtainable directly from the stream function and stress distributions already presented by applying the Newtonian limit of zero molecular relaxation time and zero concentration and using the fact that the Newtonian stress and the strain rate are linearly related by $2R_s^{-1}$.

Now that the boundary conditions have been specified the system of differential equations, consisting of the stream function equation, Eq. (2.12), the vorticity equation, Eq. (2.13), and the stress equations, Eqs. (2.14) through (2.16), can be numerically modeled.

4. Numerical Modeling of the Non-Newtonian Equations

Before the equations can be discretized, a computational grid must be established and the location of the dependent variables defined. In this investigation a Cartesian grid is defined on the x–y plane of the flow domain (see Fig. 2). In the inflow region the grid spacing is 4×10^{-2} and in the remainder of the domain the spacing is 2×10^{-2} (note that all spatial variables are scaled by $L = 1$ in.). This allows for better resolution in the contraction and outflow sections. With these spacings the inflow region has 25 grid points in the cross-stream and streamwise directions, the contraction and outflow regions have a maximum of 50 grid points in the cross-stream direction and a total of 75 grid points in the streamwise direction. At first glance it may appear advantageous to transform to the (ϕ, η) coordinate system described in Appendix A since in that system the boundary is simply another coordinate line ($\eta = 0.08$). However, as is shown in Appendix B, transforming to the (ϕ, η) system creates a mathematical singularity in the flow domain thus making this system unacceptable.

Figure 3 shows the location of the different variables on a typical square grid cell in the computational mesh.

Having defined the locations of the variables, let us first difference the stream function equation, Eq. (2.12). If the grid spacing in the x and y directions is equal, this Poisson equation can be differenced to second-order accuracy using the "5-point formula";

$$-\Delta^2\omega_{i,j} = \delta_x{}^2\psi_{i,j} + \delta_y{}^2\psi_{i,j} = \psi_{i+1,j} + \psi_{i-1,j} - 4\psi_{i,j} + \psi_{i,j+1} + \psi_{i,j-1}, \quad (4.1)$$

where $\Delta^2 (= \Delta x^2 = \Delta y^2)$ is the grid spacing squared. One of the most commonly used techniques for solving the stream function equation is the iterative method of

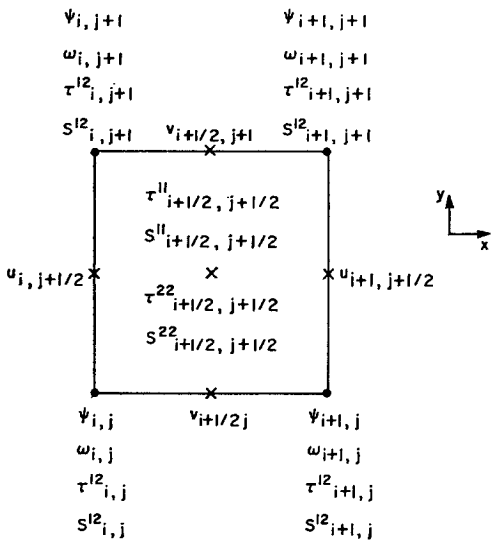

FIG. 3. Location of dependent variables in a typical grid cell.

successive overrelaxation (SOR). Using this method, one can write the algorithm for the stream function equation at the (i,j) point as

$$\psi_{i,j}^{(k+1)} = (1-\beta)\,\psi_{i,j}^{(k)} + \frac{\beta}{4}(\psi_{i+1,j}^{(k)} + \psi_{i-1,j}^{(k+1)} + \psi_{i,j+1}^{(k)} + \psi_{i,j-1}^{(k+1)} + \Delta^2\omega_{i,j}), \quad (4.2)$$

where β is the relaxation parameter (computational tests yielded an optimum $\beta \simeq 1.8$), and the superscripts in parentheses indicate iteration level. The convergence criterion used for this discretized equation (and the remaining equations) is

$$\max \left| \frac{\psi_{i,j}^{(k+1)} - \psi_{i,j}^{(k)}}{\psi_{i,j}^{(k+1)}} \right| \leqslant \epsilon, \quad (4.3)$$

where the $|\ |$ denote absolute value and $\epsilon = 10^{-7}$ for this stream function equation. The next equation to be modeled is the vorticity equation, Eq. (2.13).

A cursory look at the vorticity equation reveals that second-order centered differencing of the advection terms would yield a difference equation with no explicit dependence on the variable $\omega_{i,j}$. In addition, if one uses this type of differencing on the vorticity equation for a Newtonian fluid, it can be shown [8] that undue amplification of the truncation error in the advection term results as the Reynolds number increases. An alternative is to use unidirectional or upstream differencing of the advection terms. The major drawback of this scheme is the artificial viscosity errors due to the first-order accuracy of the difference scheme. Since the artificial viscosity errors are proportional to the mesh spacing, the effect of this error on the flow can be examined by varying the grid size. This type of check on the system can be made at the interface between the coarse (inflow region) and fine (contraction region) mesh. From the smooth variation of the variables across the interface between the two meshes, it was concluded that the artificial viscosity errors were unimportant in this region (although farther downstream in the contraction region this error was found to be significant). In addition, this is a viscous effect and the extra effect of the non-Newtonian fluid is its elastic response to the flow field and this elastic behavior would not be affected. In spite of the artificial viscosity errors it would appear from the above dicussion that upstream differencing would be best suited for this problem.

Using upstream differencing of the advection terms in Eq. (2.13) and assuming equal grid spacings, one can write the discretized form of the vorticity equation as

$$\begin{aligned}\omega_{i,j}[|u| + |v|] = 0.5\{&(|v| - v)\,\omega_{i,j+1} + (|v| + v)\,\omega_{i,j-1} \\ &+ (|u| - u)\,\omega_{i+1,j} + (|u| + u)\,\omega_{i-1,j}\} \\ &+ 2\Delta^{-1}[\delta_x{}^2\tau_{i,j}^{12} - \delta_y{}^2\tau_{i,j}^{12} + \delta_x\delta_y(\tau_{i,j}^{22} - \tau_{i,j}^{11})],\end{aligned} \tag{4.4}$$

where

$$u = \Delta^{-1}(\psi_{i,j+1} - \psi_{i,j}) = \Delta^{-1}\Delta_y\psi_{i,j}\,, \tag{4.5}$$

$$v = -\Delta^{-1}(\psi_{i+1,j} - \psi_{i,j}) = -\Delta^{-1}\Delta_x\psi_{i,j}\,, \tag{4.6}$$

Now with the form of Eq. (4.4) it would appear that SOR could be used to iterate to the solution matrix. However, the numerical experiments performed to determine the optimum relaxation parameter indicated that relaxation is destabilizing. It is thus necessary to revert to a slower (but stable) iteration method; the Gauss–Seidel method was tested and found acceptable. Using this method, one obtains from Eq. (4.4)

$$\begin{aligned}\omega_{i,j}^{(k+1)} = 0.5[|u| + |v|]^{-1}\{&(|v| - v)\,\omega_{i,j+1}^{(k)} \\ &+ (|v| + v)\,\omega_{i,j-1}^{(k+1)} + (|u| - u)\,\omega_{i+1,j}^{(k)} \\ &+ (|u| + u)\,\omega_{i-1,j}^{(k+1)} + 2\Delta^{-1}[\delta_x{}^2\tau_{i,j}^{12} \\ &- \delta_y{}^2\tau_{i,j}^{12} + \delta_x\delta_y(\tau_{i,j}^{22} - \tau_{i,j}^{11})]\}.\end{aligned} \tag{4.7}$$

Here the stresses are taken as fixed forcing functions in the iteration of Eq. (4.7). The iterations continue until the convergence criterion analogous to Eq. (4.3), with $\epsilon = 10^{-5}$, is met. It should be noted that along the solid boundary it would be necessary to know the vorticity at the wall, which for the straight sections in the inflow and outflow regions is given by Eq. (3.11) and (3.13). The difference approximation to this equation can be found by expanding $\psi_{i,j=J+1}$ about the boundary $j = J$ and, using the no-slip condition to obtain

$$\omega_{i,J} = \frac{2(\psi_{i,J} - \psi_{i,J-1})}{\Delta y^2} + O(\Delta y). \tag{4.8}$$

In addition, in the iteration procedure this wall value is held constant. Let us now difference the constitutive equations.

Since the viscoelastic constitutive equations exhibit elastic propagation behavior, it would be desirable to maintain the transportive property, at least in connection with the stress advection terms. Then applying the Gauss–Seidel method (relaxation methods proved to be destabilizing) to the first-order difference approximations to Eqs. (2.14) through (2.16), one finds the following algorithms for $\tau^{12}_{i,j}$, $\tau^{11}_{i+\frac{1}{2},j+\frac{1}{2}}$ and $\tau^{22}_{i+\frac{1}{2},j+\frac{1}{2}}$, with the stress advection terms upstream differenced and the strain rate advection terms centered differenced,

$$\begin{aligned}
\tau^{12(k+1)}_{i,j} = {} & [1 + \lambda_1(|u| + |v|)_{i,j}\,\Delta^{-1}]^{-1}\Big\{\lambda_1\Big[\Big(\frac{|v| - v}{2\Delta}\Big)_{i,j}\tau^{12(k)}_{i,j+1} \\
& + \Big(\frac{|v| - v}{2\Delta}\Big)_{i,j}\tau^{12(k+1)}_{i,j-1} + \Big(\frac{|u| - u}{2\Delta}\Big)_{i,j}\tau^{12(k)}_{i+1,j} + \Big(\frac{|u| + u}{2\Delta}\Big)_{i,j}\tau^{12(k+1)}_{i-1,j} \\
& + \Big(S^{12} - \frac{\omega}{2}\Big)_{i,j}\Big(\frac{\tau^{22(k)}_{i+\frac{1}{2},j+\frac{1}{2}} + \tau^{22(k+1)}_{i+\frac{1}{2},j-\frac{1}{2}} + \tau^{22(k+1)}_{i-\frac{1}{2},j+\frac{1}{2}} + \tau^{22(k+1)}_{i-\frac{1}{2},j-\frac{1}{2}}}{4}\Big) \\
& + \Big(S^{12} + \frac{\omega}{2}\Big)_{i,j}\Big(\frac{\tau^{11(k)}_{i+\frac{1}{2},j+\frac{1}{2}} + \tau^{11(k+1)}_{i+\frac{1}{2},j-\frac{1}{2}} + \tau^{11(k+1)}_{i-\frac{1}{2},j+\frac{1}{2}} + \tau^{11(k+1)}_{i-\frac{1}{2},j-\frac{1}{2}}}{4}\Big)\Big] \\
& \times \frac{2(1 + c[\eta])}{R_s}S^{12}_{i,j} + \frac{2\lambda_1}{R_s}\Big[\frac{u_{i,j}\mu_x\delta_x S^{12}_{i,j}}{\Delta} \\
& + \frac{v_{i,j}\mu_y\delta_y S^{12}_{i,j}}{\Delta} - \Big(S^{12} - \frac{\omega}{2}\Big)_{i,j}\mu_x\mu_y S^{22}_{i,j} - \Big(S^{12} + \frac{\omega}{2}\Big)_{i,j}\mu_x\mu_y S^{11}_{ij}\Big]\Big\},
\end{aligned} \tag{4.9}$$

$$\begin{aligned}
\tau^{11(k+1)}_{i+\frac{1}{2},j+\frac{1}{2}} = {} & [1 + \lambda_1(|u| + |v|)_{i+\frac{1}{2},j+\frac{1}{2}}\,\Delta^{-1} \\
& - 2\lambda_1 S^{11}_{i+\frac{1}{2},j+\frac{1}{2}}]^{-1}\Big\{\lambda_1\Big(\frac{|v| - v}{2\Delta}\Big)_{i+\frac{1}{2},j+\frac{1}{2}}\tau^{11(k)}_{i+\frac{1}{2},j+\frac{3}{2}} \\
& + \Big(\frac{|v| + v}{2\Delta}\Big)_{i+\frac{1}{2},j+\frac{1}{2}}\tau^{11}_{i+\frac{1}{2},j-\frac{1}{2}} + \Big(\frac{|u| - u}{2\Delta}\Big)_{i+\frac{1}{2},j+\frac{1}{2}}\tau^{11(k)}_{i+\frac{3}{2},j+\frac{1}{2}}
\end{aligned}$$

$$+\left(\frac{|u|+u}{2\Delta}\right)\tau^{11(k+1)}_{i-\frac{1}{2},j+\frac{1}{2}}+2\mu_x\mu_y\left(S^{12}-\frac{\omega}{2}\right)_{i+\frac{1}{2},j+\frac{1}{2}}$$

$$\times\left(\frac{\tau^{12}_{i+1,j+1}+\tau^{12(k)}_{i+1,j}+\tau^{12(k)}_{i,j+1}+\tau^{12(k+1)}_{i,j}}{4}\right)\Big]$$

$$+\frac{2(1+c[\eta])}{R_s}S^{11}_{i+\frac{1}{2},j+\frac{1}{2}}+\frac{2\lambda_1}{R_s}\Big[u_{i+\frac{1}{2},j+\frac{1}{2}}\frac{\mu_x\delta_x S^{11}_{i+\frac{1}{2},j+\frac{1}{2}}}{\Delta}$$

$$+v_{i+\frac{1}{2},j+\frac{1}{2}}\frac{\mu_y\delta_y S^{11}_{i+\frac{1}{2},j+\frac{1}{2}}}{\Delta}-2\mu_x\mu_y\left(S^{12}-\frac{\omega}{2}\right)_{i+\frac{1}{2},j+\frac{1}{2}}(\mu_x\mu_y S^{12}_{i+\frac{1}{2},j+\frac{1}{2}})$$

$$-2(S^{11}_{i+\frac{1}{2},j+\frac{1}{2}})^2\Big]\Big\}, \tag{4.10}$$

$$\tau^{22(k+1)}_{i+\frac{1}{2},j+\frac{1}{2}}=[1+\lambda_1(|u|+|v|)_{i+\frac{1}{2},j+\frac{1}{2}}\Delta^{-1}$$

$$-2\lambda_1 S^{22}_{i+\frac{1}{2},j+\frac{1}{2}}]^{-1}\Big\{\lambda_1\Big[\left(\frac{|v|-v}{2\Delta}\right)_{i+\frac{1}{2},j+\frac{1}{2}}\tau^{22(k)}_{i+\frac{3}{2},j+\frac{1}{2}}$$

$$+\left(\frac{|v|+v}{2\Delta}\right)_{i+\frac{1}{2},j+\frac{1}{2}}\tau^{22(k+1)}_{i+\frac{1}{2},j-\frac{1}{2}}+\left(\frac{|u|-u}{2\Delta}\right)_{i+\frac{1}{2},j+\frac{1}{2}}\tau^{22(k)}_{i+\frac{3}{2},j+\frac{1}{2}}$$

$$+\left(\frac{|u|+u}{2\Delta}\right)_{i+\frac{1}{2},j+\frac{1}{2}}\tau^{22(k+1)}_{i-\frac{1}{2},j+\frac{1}{2}}+2\mu_x\mu_y\left(S^{12}+\frac{\omega}{2}\right)_{i+\frac{1}{2},j+\frac{1}{2}}$$

$$\times\left(\frac{\tau^{12(k)}_{i+1,j+1}+\tau^{12(k)}_{i+1,j}+\tau^{12(k)}_{i,j+1}+\tau^{12(k+1)}_{i,j}}{4}\right)\Big]$$

$$+\frac{2(1+c[\eta])}{R_s}S^{22}_{i+\frac{1}{2},j+\frac{1}{2}}+\frac{2\lambda_1}{R_s}\Big[u_{i+\frac{1}{2},j+\frac{1}{2}}\frac{\mu_x\delta_x S^{22}_{i+\frac{1}{2},j+\frac{1}{2}}}{\Delta}$$

$$+v_{i+\frac{1}{2},j+\frac{1}{2}}\frac{\mu_y\delta_y S^{22}_{i+\frac{1}{2},j+\frac{1}{2}}}{\Delta}-2\mu_x\mu_y\left(S^{12}+\frac{\omega}{2}\right)_{i+\frac{1}{2},j+\frac{1}{2}}(\mu_x\mu_y S^{12}_{i+\frac{1}{2},j+\frac{1}{2}})$$

$$-2(S^{22}_{i+\frac{1}{2},j+\frac{1}{2}})^2\Big]\Big\}, \tag{4.11}$$

where

$$\mu_x\mu_y S^{11}_{i,j}=\frac{S^{11}_{i+\frac{1}{2},j+\frac{1}{2}}+S^{11}_{i+\frac{1}{2},j-\frac{1}{2}}+S^{11}_{i-\frac{1}{2},j+\frac{1}{2}}+S^{11}_{i-\frac{1}{2},j-\frac{1}{2}}}{4},$$

$$\mu_x\delta_x S^{12}_{i,j}=\frac{S^{12}_{i+1,j}-S^{12}_{i-1,j}}{2},\qquad v_{i,j}=\frac{-\mu_x\delta_x\psi_{i,j}}{2},$$

$$u_{i,j}=\frac{\mu_y\delta_y\psi_{i,j}}{\Delta},\qquad u_{i+\frac{1}{2},j+\frac{1}{2}}=\frac{\mu_x\Delta_y\psi_{i+\frac{1}{2},j}}{\Delta},$$

$$v_{i+\frac{1}{2},j+\frac{1}{2}}=-\frac{\mu_y\Delta_x\psi_{i,j+\frac{1}{2}}}{\Delta},$$

$$\left(S^{12}+\frac{\omega}{2}\right)_{i+\frac{1}{2},j+\frac{1}{2}}=\frac{1}{4}\left[\left(S^{12}+\frac{\omega}{2}\right)_{i+1,j+1}+\left(S^{12}+\frac{\omega}{2}\right)_{i+1,j}\right.$$
$$\left.+\left(S^{12}+\frac{\omega}{2}\right)_{i,j+1}+\left(S^{12}+\frac{\omega}{2}\right)_{i,j}\right],$$

$$\left(S^{12}-\frac{\omega}{2}\right)_{i+\frac{1}{2},j+\frac{1}{2}}=\frac{1}{4}\left[\left(S^{12}-\frac{\omega}{2}\right)_{i+1,j+1}+\left(S^{12}-\frac{\omega}{2}\right)_{i+1,j}\right.$$
$$\left.+\left(S^{12}-\frac{\omega}{2}\right)_{i,j+1}+\left(S^{12}-\frac{\omega}{2}\right)_{i,j}\right]$$

$$S^{12}_{i,j}=\tfrac{1}{2}(\delta_y{}^2-\delta_x{}^2)\,\psi_{i,j}\,,$$

$$S^{11}_{i+\frac{1}{2},j+\frac{1}{2}}=-S^{22}_{i+\frac{1}{2},j+\frac{1}{2}}=\Delta_x\Delta_y\psi_{i,j}\,,$$

and variables without superscripts are taken as fixed in the inner iteration. Note that the discretized strain rate equations are center differenced with respect to their grid locations and that in the Newtonian limit the shear and normal stress difference approximations also become second-order accurate with respect to their grid locations. In addition, from Eqs. (4.9) through (4.11), it is seen that each variable is calculated successively at each point in the computational mesh; that is, for each node point location (i, j) the τ^{12} shear stress is calculated first, then at the corresponding cell center $(i+\frac{1}{2}, j+\frac{1}{2})$ the normal stresses τ^{11} and τ^{22} are calculated. In this way, after one sweep through the entire mesh each variable has been calculated once with the strain rates, vorticity and stream function fixed variables. Since the stress boundary conditions are not as straightforward as the vorticity and stream function, it is advantageous to examine their difference approximations in some detail.

Along the centerline the shear stress condition poses no problem since it is zero there; however, as was discussed in the previous section, the normal stresses will be troublesome. Referring to Eqs. (4.10) and (4.11), one can see that for these normal stress values to be used the v-velocity must be positive. Since this is never the case it is unnecessary to explicitly specify the normal stress values along the centerline. At the entrance to the domain the stress conditions are given by Eqs. (3.15) through (3.17). The discretized shear stress distribution is easily specified since the S^{12} strain rate distribution at the entrance can be directly obtained from the known stream function distribution (3.1). The discretized τ^{11} normal stress distribution along the entrance is found in a similar manner because of the simple relationship to S^{12}, and, of course, the discretized τ^{22} normal stress distribution is trivial. Now recall that the normal stresses are defined at the center of a grid cell, one-half mesh spacing downstream from the entrance, and note that the above conditions are applicable at the entrance. It is necessary then to use Eqs. (4.10) and (4.11) to solve for $\tau^{11}_{\frac{1}{2},j+\frac{1}{2}}$ and $\tau^{22}_{\frac{1}{2},j+\frac{1}{2}}$, knowing the stress distribution one-half mesh spacing upstream. Due to the nature of the flow at the exit, the stress conditions there were handled in the same manner as the stress entrance conditions since the differential formulation of the two sets of conditions were the same. The only difference here is that the S^{12} strain rate is based on a cal-

culated discrete distribution of velocity values at the exit, whereas at the entrnace the velocity distribution was a specified continuous distribution. Along the straight solid boundaries, the specification of the discretized stress condition, once again given by Eqs. (3.15) through (3.17), is more direct. Using the conditions of zero normal and tangential velocities, one finds for the stress conditions there

$$\tau^{12}_{i,J} = 2(1 + c[\eta])\, R_s^{-1} \Delta^{-2}(\psi_{i,J-1} - \psi_B), \tag{4.12}$$

$$\tau^{11}_{i,J} = 8\lambda_1 c[\eta]\, R_s^{-1} \Delta^{-2}[\psi_{i,J-1} - \psi_B]^2, \tag{4.13}$$

$$\tau^{22}_{i,J} = 0.0. \tag{4.14}$$

Up to this point the equations have been discretized using equal grid spacings; however, at the points adjacent to the curved boundary, unequal spacing occurs and the form of the difference equations changes slightly.

First, consider the stream function equation, Eq. (2.12). It will be sufficient here to consider unequal spacings in only one direction. For example, in the x-direction, if the functions $\psi(x_+, y)$ and $\psi(x - \Delta x, y)$ (or $\psi_{+,j}$ and $\psi_{i-1,j}$) are expanded about the point $\psi(x, y)(\psi_{i,j})$ and the resulting series expansions solved simultaneously for ψ_{xx}, the following first-order difference equation results:

$$\psi_{xx} = \frac{2(\Delta_+\psi_{i,j}\, \nabla x - \nabla\psi_{i,j}\, \Delta_+ x)}{(\Delta_+ x)^2\, \nabla x + \Delta_+ x(\nabla x)^2}, \tag{4.15}$$

where

$$\Delta_+\psi_{i,j} = \psi_{+,j} - \psi_{i,j}, \quad \nabla\psi_{i,j} = \psi_{i,j} - \psi_{i-1,j},$$

and $\psi_{+,j} = 1.0$. If the spacing is irregular in the y-direction or irregular in both directions the appropriate finite-difference expressions for the derivatives would be used in discretizing the stream function equation. Nevertheless, no matter what discretized form of the stream equation is used one can always solve for $\psi_{i,j}$ and obtain an equation analogous to Eq. (4.2) with the same β.

Now consider the vorticity equation, Eq. (2.13), at points adjacent to the curved boundary. In this equation the vorticity derivatives only appear in the advection terms and due to the upstream differencing the finite-difference approximations are only first-order accurate even with equal grid spacings. The simplest first-order-accurate forward difference approximation to these derivatives for the irregular grid spacing, in the x-direction, for example, can be easily written as

$$\omega_x = (\omega_{+,j} - \omega_{i,j})/\Delta_+ x. \tag{4.16}$$

Since the irregular spacing occurs only at the curved boundary the value of $\omega_{+,j}$ (or $\omega_{i,+}$) must be determined from the discretized form of Eq. (3.12). In addition, from Eq. (2.13), it would also appear that the stress derivatives at the points adjacent to the boundary would have to be discretized using unequal grid spacings. However,

numerical experiments indicated that if the grid system extended beyond the solid boundary (see Fig. 4) stress values at the exterior points could be found making it unnecessary to use irregular differences at the curved boundary for the stress derivatives. Therefore, in order to solve the vorticity equation at points adjacent (interior) to the curved boundary it is necessary to know the value of the vorticity on the boundary and the stresses exterior to the boundary. Along the curved boundary the vorticity is defined by Eq. (3.12). Following a procedure similar to that used in deriving Eq. (4.8), but now expanding about the boundary in the η-direction along a line of constant ϕ, the discretized form of (3.12) can be written as

$$\omega = 4(\phi^2 + (0.08)^2)(1.0 - \psi_{\phi,\eta_-})(0.08 - \eta_-)^{-2}, \tag{4.17}$$

where η_- is a coordinate location interior to the boundary. Now let us consider the stresses exterior to the boundary.

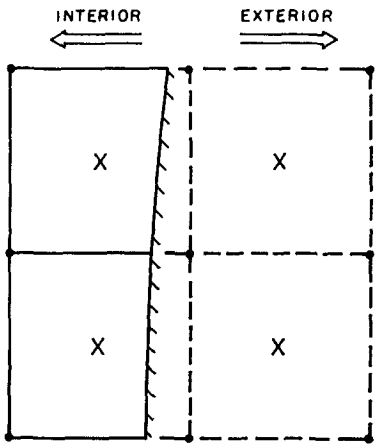

FIG. 4. Grid cell structure adjacent to solid boundary.

It is necessary to know the Cartesian values of the stresses outside the boundary; however, along the curved boundary any symmetry statements about the variables are with respect to the $\phi - \eta$ system. Therefore, exterior to the boundary the transformation law equation (3.22) is needed, and interior to the boundary it is necessary to know the stresses in the $\phi - \eta$ system. Since the stress values in the interior of the flow are known with respect to a Cartesian frame these values must be transformed to the curvilinear system. In equation form the above two statements can be written as

$$^{e}\tau^{ij} = X_k{}^{j} X_i{}^{l}\, {}^{e}\tau(l, k) \tag{4.18}$$

and

$${}^{i}\tau(l, k) = X,{}^{k} X_l{}^{i}\, {}^{i}\tau^{ij}, \tag{4.19}$$

where the superscripts on the left of the stresses denote exterior and interior. The problem that remains is to relate ${}^{e}\tau(l, k)$ to ${}^{i}\tau(l, k)$ along a line of constant ϕ.

Due to the complexity of the constitutive equations it is necessary to resort to a qualitative argument to determine the proper symmetry conditions across the boundary. Such arguments must assume that very near the wall, curvature effects are small thus making the stream function values across the boundary, along a line of constant ϕ, symmetric to second order and, the normal and tangential velocities approach zero. In the previous section the wall stress conditions were found to correspond to the stress equations valid along the centerline of a parallel flow. In this type of flow the conditions on either side of the "centerline" (wall) for the non-Newtonian shear stress and nonzero normal stress (both are related to $S(\phi, \eta)$) are clear. Both the stresses are symmetric and in equation form can be written for the ϕ–η system as

$$^{e}\tau(\phi, \eta) = \frac{g^{22}|_{\text{interior}}}{g^{22}|_{\text{exterior}}} {}^{i}\tau(\phi, \eta), \tag{4.20}$$

$$^{e}\tau(\phi, \phi) = \frac{g^{22}|_{\text{interior}}}{g^{22}|_{\text{exterior}}} {}^{i}\tau(\phi, \phi), \tag{4.21}$$

where the coefficient is due to the use of physical components. The condition on the remaining normal stress $\tau(\eta, \eta)$ does not appear to be obtainable from this analogy; however, since this stress component is zero along the boundary (as it would be even in the Newtonian limit) it is safe to assume that $\tau(\eta, \eta)$ is antisymmetric across the boundary

$$^{e}\tau(\eta\eta) = \frac{-g^{22}|_{\text{int}}}{g^{22}|_{\text{ext}}} {}^{i}\tau(\eta\eta). \tag{4.22}$$

Now Eqs. (4.18) and (4.19) can be used and the calculated Cartesian stresses substituted into the vorticity equation. A comment concerning Eq. (4.19) is in order. As can be seen from Fig. 4 it is very unlikely that the interior stress points needed in that equation will lie along a line of constant x or y in the Cartesian system. It is thus necessary to use two-way linear interpolation [9] from the nearest Cartesian stresses, which are defined at interior node points, to determine the appropriate stress values to be used in Eq. (4.19). Of course the validity of such an approximation can only be determined by numerical experiments. The numerical tests on this approximation were satisfactory, giving vorticity values which were both uniform and consistent near the curved boundary. Even with the above irregular differencing and the necessity to go outside the boundary for the stresses, it is still a small matter of algebra to solve for $\omega_{i,j}$ and form an equation similar to Eq. (4.7). Finally, let us examine the constitutive equations, Eqs. (2.14) through (2.16), at points adjacent to the curved boundary.

The first-order difference approximations, for unequal grid spacing, of the stress derivatives are similar to those for the vorticity, with the strain rate derivatives handled in an analogous manner. These difference approximations require the values of the strain rates and stresses along the curved boundary, which can be obtained from Eqs. (3.25) through (3.27). The discretized forms of these equations yield the following values of the stresses:

$$\tau_B^{12} = 4\phi(1 + c[\eta])\, R_s^{-1}\left(\frac{\psi_{\phi,\eta-} - \psi_B}{\Delta^2}\right) - 1.28(\phi^2 + (0.08)^2)^{1/2}\lambda_1 c[\eta]\, R_s^{-1}\left(\frac{\psi_{\phi,\eta-} - \psi_B}{\Delta^2}\right)^2, \tag{4.23}$$

$$\tau_B^{11} = 0.32(1 + c[\eta])\, R_s^{-1}\left(\frac{\psi_{\phi,\eta-} - \psi_B}{\Delta^2}\right) + 16(\phi^2 + (0.08)^2)^{1/2}(\phi + (\phi^2 + (0.08)^2)^{1/2})\,\lambda_1 R_s^{-1} c[\eta]\left(\frac{\psi_{\phi,\eta-} - \psi_B}{\Delta^2}\right)^2, \tag{4.24}$$

$$\tau^{22} = -0.32(1 + c[\eta])\, R_s^{-1}\left(\frac{\psi_{\phi,\eta-} - \psi_B}{\Delta^2}\right) + 16(\phi^2 + (0.08)^2)^{1/2}(-\phi + (\phi^2 + (0.08)^2)^{1/2})\,\lambda_1 R_s^{-1} c[\eta]\left(\frac{\psi_{\phi,\eta-} - \psi_B}{\Delta^2}\right)^2, \tag{4.25}$$

where

$$\psi_B = 1.0.$$

Having specified the non-Newtonian stress boundary conditions, one can easily obtain the strain rate boundary conditions. Recall that in the Newtonian limit of zero molecular relaxation time and zero concentration the non-Newtonian stresses reduce to the Newtonian stress values. Since the Newtonian stress values are linearly related to the strain rate values by $R_s/2$, the boundary values for the strain rate can be easily obtained from Eqs. (4.23) through (4.25). Now that the equations for the stream function, vorticity, strain rates, and stresses have been differenced along with the specification of the discretized boundary conditions, it is necessary to place these equations in sequences to form an outer iteration loop.

Since the Newtonian values of all the flow variables are known for this contraction [1], these values were used as starting conditions in this non-Newtonian problem. The stress equations, Eqs. (4.9) through (4.11), were iterated first (an inner iteration) using the Newtonian values. The new stress values obtained from the iterated stress equations were used in the vorticity equation. Along with these new stress values, the previously calculated stream function values and appropriate boundary conditions were used in the calculation of the vorticity. However, before these new vorticity values could be used in the stream function equation, it was necessary to use a weighted average on the calculated vorticity values [10] that is

$$\omega_{i,j} = \kappa\omega_{i,j|\text{outer iteration } k} + (1 - \kappa)\,\omega_{i,j|\text{outer iteration } k+1}, \tag{4.26}$$

where κ is a variable weighting factor. These weighted vorticity values were then used in the iteration of the stream function equation. Finally the iterated stream function values were used to obtain the strain rate values (no iterations). This entire

process formed one outer iteration loop. It should be pointed out that the coupling of these equations is rather weak, for example, the stress terms in the vorticity equation are held fixed throughout the iteration of that equation. This of course causes a slower convergence of the outer iteration loop but from numerical tests was found to be a stable computational system. The outer iteration process was continued until the following convergence criteria were met:

$$\left(1.0 - \frac{\gamma^{(\alpha)}_{i,j|\text{outer iteration } k}}{\gamma^{(\alpha)}_{i,j|\text{outer iteration } k+1}}\right) \leqslant \epsilon^{(\alpha)}, \tag{4.27}$$

where

$$\gamma^{(\alpha)}_{i,j} = \begin{Bmatrix} \psi_{i,j} & \alpha = 1 & 10^{-5} \\ \omega_{i,j} & \alpha = 2 & 10^{-3} \\ \tau^{12}_{i,j} & \alpha = 3 & 10^{-7} \\ \tau^{11}_{i+\frac{1}{2},j+\frac{1}{2}} & \alpha = 4 & 10^{-7} \\ \tau^{22}_{i+\frac{1}{2},j+\frac{1}{2}} & \alpha = 5 & 10^{-7} \end{Bmatrix} = \epsilon^{(\alpha)}.$$

5. Computational Results

Before presenting some of the non-Newtonian results it is first necessary to specify the solvent Reynolds number R_s, the concentration c, the intrinsic viscosity $[\eta]$ (note that the concentration and intrinsic viscosity always appear as $c[\eta]$) and the molecular relaxation time λ_1. Let us choose as an example a value for R_s of 5000 [1], which corresponds to an entrance velocity of 20 cm/sec, based on the previously defined length scale and the viscosity of water ($=10^{-2}$cm^2/sec). An estimate for the value of $c[\eta]$ can best be found by considering the polymer Poly(ethylene oxide), or Polyox (WSR-301). The intrinsic viscosity for this polymer has been found to be approximately 20 dl/g [11]. Normally the intrinsic viscosity is dependent on shear but here it is assumed constant. Experimental results (11) indeed show that the intrinsic viscosity is relatively constant at concentrations of the order of 50 ppm (parts per million by weight) and below. Thus for Polyox at this concentration the term $c[\eta]$ would be of the order of 10^{-1}. Numerical tests indicated, however, that for $c[\eta] = 0.1$ there was only a slight change in the magnitude of the variables relative to Newtonian starting values. It was decided that a more interesting value would be $c[\eta] = 1.0$, which would effectively raise the stress levels by a factor of 2. Since the Reynolds number R_s and the term $c[\eta]$ have been specified, the only remaining parameter to be set is λ_1. Two values of λ_1 were tested : $\lambda_1 = 5.0 \times 10^{-3}$ and 9.0×10^{-3}. The difference in the behavior of the flow variables between the two parameters was rather slight and only the larger value of λ_1 ($= 9.0 \times 10^{-3}$) will be presented here. Having specified the Reynolds number, we can examine the behavior of the flow

The stream function contours are presented in Fig. 5a. Since the motion is steady the streamlines represent the paths (streaklines) that tracer elements would follow if

injected into the flow. Due to the deceleration of the streamwise velocity near the solid boundary in the inflow region, the flow separates and, as is clearly seen, a large recirculation region develops in the corner. A picture of relative velocity magnitude and direction can also be seen from this figure by noting the equispaced stream function values. At the entrance to the domain the stream function values clearly indicate the relative magnitude of the velocities across the entrance (the velocity being given by 0.2/(spatial distance between neighboring streamlines of equal separation)).

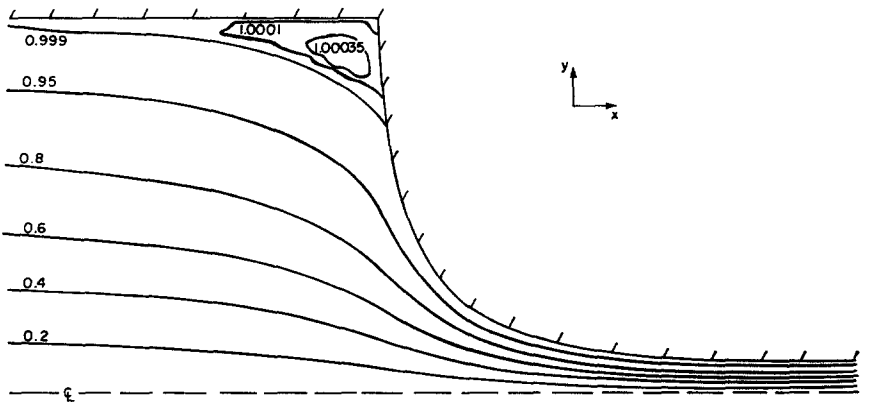

FIG. 5a. Stream function contour lines for the non-Newtonian fluid.

For example, the distance between the centerline and $\psi = 0.2$ is approximately one-third the distance between $\psi = 0.8$ and $\psi = 1.0$; hence the average total velocity near the centerline is about three times as large as the average total velocity in the vicinity of the wall. At the exit of the domain the picture has changed; using the same two streamlines one finds that the distances are now in a ratio of about three to two. What has happened is the velocity profile has become more blunted at the exit and if allowed to continue downstream would eventually evolve to a parabolic profile over the width of the region. This streamwise variation is rather weak and computational checks, by extending the outflow region father downstream, on the assumption of a fully developed flow showed that the results upstream of the exit were not affected. Comparison of these results with the corresponding Newtonian streamlines (Fig. 5b) indicates that the flow has not changed throughout most of the domain; the only change that has occurred is in the size of the recirculation region in the corner of the domain. As can be seen this recirculation region has gotten smaller. This means that the separation point has moved farther downstream; implying that the non-Newtonian fluid velocity must not have decelerated as quickly as the Newtonian velocity [1]. The reason for this slower deceleration is the increased elasticity effects as retardation time, given here by $\lambda_1(1 + c[\eta])^{-1}$, increases [1]. If a change in the flow occurred in the inflow, some sort of change in the flow should occur near the wall in the lower part of the domain. Unfortunately, it was here, near the wall, that artificial viscosity effects

dominated, thus prohibiting any elastic effects from the constitutive equations to affect the flow.

In Fig. 6 isovorticity lines are plotted for the non-Newtonian fluid. As expected from the comparison of both Newtonian and non-Newtonian stream function contours, there was no variation from the Newtonian behavior except in the corner region, and even here the change was slight. It will be shown shortly that in the

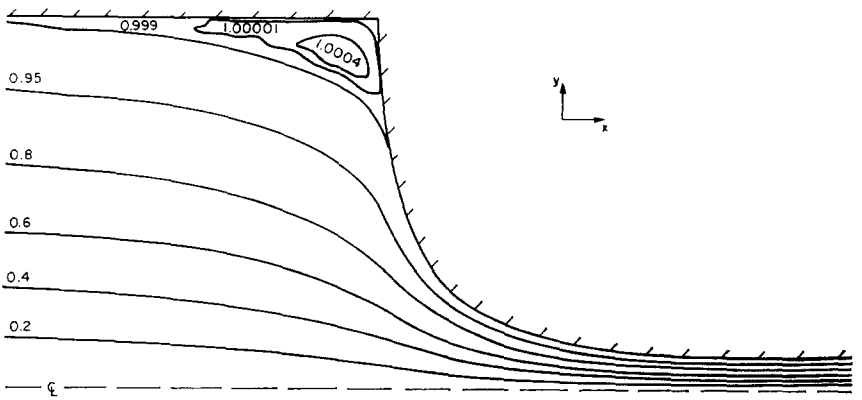

FIG. 5b. Stream function contour lines for the Newtonian fluid.

contraction region these contours provide an estimate of the boundary layer thickness. In addition, the boundary layer thickness is related to the magnitude of the artificial viscosity errors present in the computation. To see this let us briefly look at the velocity at a cross section of the contraction region; in particular, consider the point $x = 1.7$ downstream from the domain entrance (Fig. 7), since in this region of the contraction estimates on the boundary layer thickness can be made more precise due to the uniform deformation rate [1]. The displacement thickness δ^* can be estimated

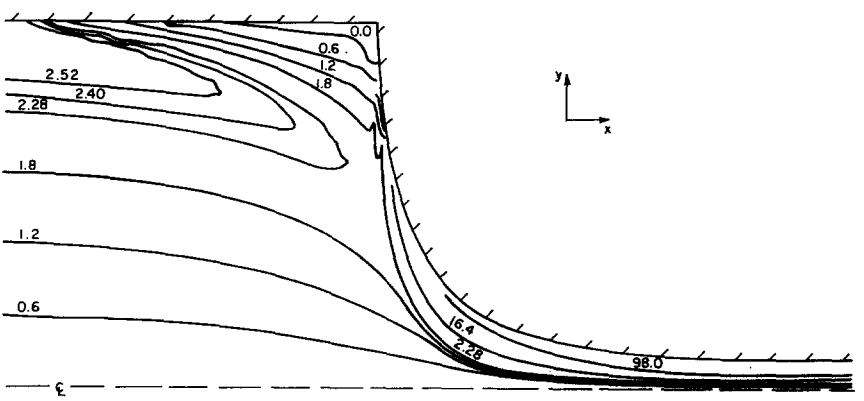

FIG. 6. Vorticity contour lines for the non-Newtonian fluid.

by calculating the area under the curves in Fig. 6 and dividing by the external mean velocity. This calculation then yields a displacement thickness of $\delta^* = 0.0205$. As a check on this computational result recall that for a linearly increasing free stream velocity (which is the case along the centerline of this contraction) the displacement thickness would be like $\delta^* \sim (R_s \psi_{xy})^{-1/2}$. (Notice here that this expression is rather vague as to a choice of multiplicative constant; if the above flow is likened to stagnation point flow then the appropriate constant is 0.65. However, for our purposes here the above expression will suffice.) Along the centerline at $x = 1.7$, ψ_{xy} is found to be equal to 15.0 thus the value of δ^* is about 0.00365. As can be seen the

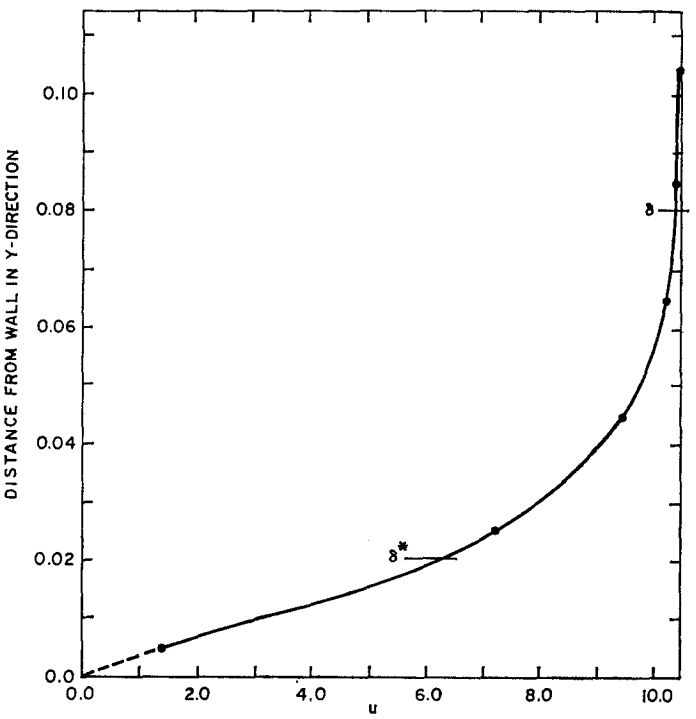

FIG. 7. Velocity profile across contraction at $x = 1.7$.

computational and theoretical estimates of δ^* differ by a factor of 6. This discrepancy can be explained by taking into account the effect of numerical viscosity. As a rough estimate of the additional viscous effect let us assume the error produced by the upstream differencing of the advection terms was of the order of $v\Delta/2$, where Δ is the grid spacing ($= 2 \times 10^{-2}$) and v is some local velocity. Taking $v = 3.0$ as a local characteristic velocity near the wall, one finds that the numerical viscosity is 3.0×10^{-2} (which corresponds to a computational Reynolds number of $R_c = 33.0$). Now letting $\delta^* \sim (R_{c\psi xy})^{-1/2}$ this new estimate gives a value of 0.0477 for the displacement thickness, which is more in line with the computational result. It thus appears that

computational viscosity does indeed play a significant role in this region of the flow domain. Finally, from Fig. 7, if we assume that the boundary layer thickness δ is about four times as large as the displacement thickness (as is the case for stagnation point flows) the computational results indicate that $\delta \simeq 0.08$. Thus, returning to Fig. 6, it would appear the isovorticity lines emanating from the contraction wall tend to outline a region whose width is the boundary layer thickness δ. It should be noted at this point that attempts to use values of λ_1 greater than 9.5×10^{-3} (corresponding to a maximum $2S\lambda_1 \simeq 0.3$) resulted in instabilities in the stress equations. These instabilities may be attributed to a possible decoupling of the stress equations from the vorticity equation because of the artificial viscosity errors, or to the method of solution. Even though this is a steady-state method it may introduce time-like instabilities into the problem. This type of instability can be shown to occur for a one-dimensional model transport equation [12]. Let us now consider the stress contours.

In Fig. 8a the τ^{12} shear stress contours are plotted. An interesting check on these results is to see if the point of separation, as taken from the non-Newtonian stream function plot, corresponds to the point of zero wall shear [13]. Comparison of Fig. 8a

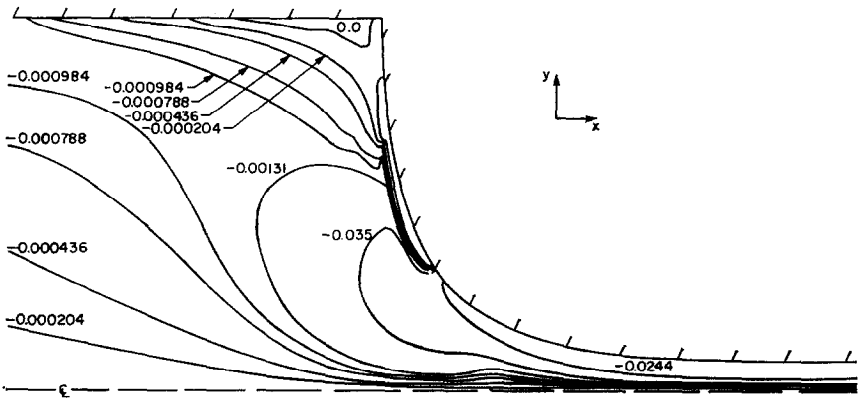

FIG. 8a. Shear stress contour lines for the non-Newtonian fluid.

with Fig. 5a indicates that the two points are in fact very close. An additional observation about the stress levels can be made on the basis of estimates of boundary layer size and effects of computational viscosity. It was found in estimating the boundary layer thickness that the appropriate Reynolds number should be based on the numerical viscosity $v\Delta/2$; this would imply that the stress levels here are indeed very small and have little effect on the vorticity dynamics. Comparison of the Newtonian (Fig. 8b) and non-Newtonian shear stress contours indicates that there is very little qualitative change between the two plots. This is consistent with the fact that the boundary conditions are essentially Newtonian conditions with an extra factor of $(1 + c[\eta])$, which accounts for the quantitative change in the shear stress contours. Therefore, the shearing forces in the flow are not significantly altered for this type of non-Newtonian fluid. Finally, let us examine the normal stress contours.

The τ^{11} and τ^{22} normal stress contours are plotted in Figs. 9 and 10, respectively. Comparison of the two figures clearly indicates the additional effects on the flow due to the presence of the molecules. In the inflow region of the flow domain both sets of contours are similar and divide the domain into two regions: a region closer to the centerline where the flow is accelerating downstream and a region closer to the solid

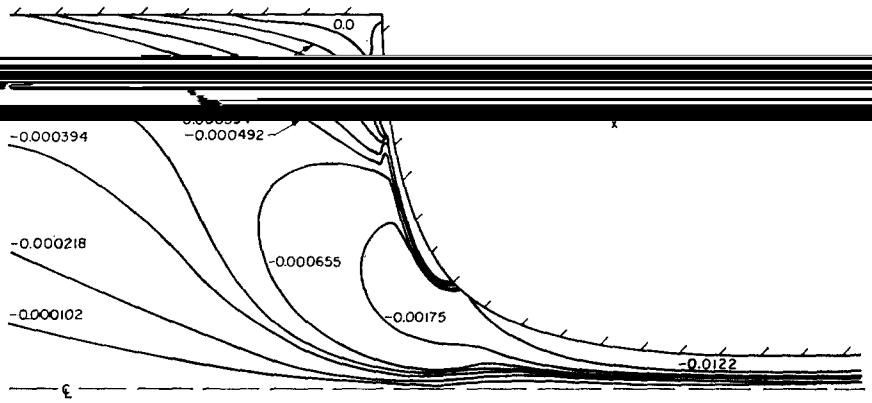

FIG. 8b. Shear stress contour lines for the Newtonian fluid.

wall where the flow is decelerating. In fact the confluence of the τ^{22} stress contours roughly indicates the growth of the boundary layer downstream through the contraction. However, in the contraction region, the qualitative behavior of the τ^{11} stress contours has changed substantially from that of the τ^{22} stress contours. This qualitative change can be explained if one notes that in this region the molecules have aligned themselves with the principal axes of strain rate, with the deviation from the axes being a function of vorticity [14]. Hence, the qualitative nature of the τ^{11} normal stress,

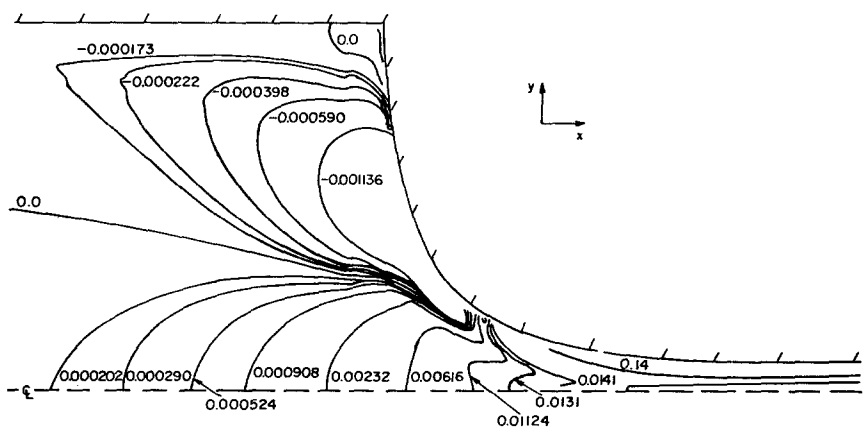

FIG. 9. τ^{11} normal stress contour lines for the non-Newtonian fluid.

at least the molecular contribution, should be similar to the behavior of the strain rate eigenvalues, the extent by which the two are similar being a function of alignment with the principal axes. In addition, if one compares these non-Newtonian contours with the Newtonian τ^{11} normal stress contours in Fig. 11 (recall for a Newtonian fluid $\tau^{11} = -\tau^{22}$) it is seen that the non-Newtonian τ^{11} contours are qualitatively

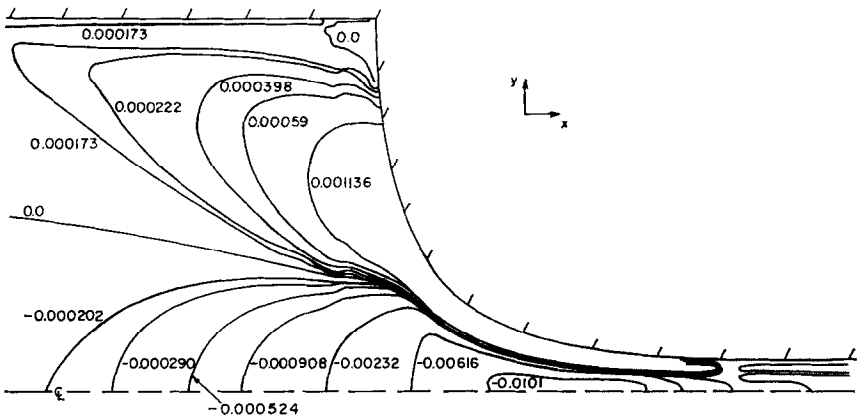

FIG. 10. τ^{22} normal stress contour lines for the non-Newtonian fluid.

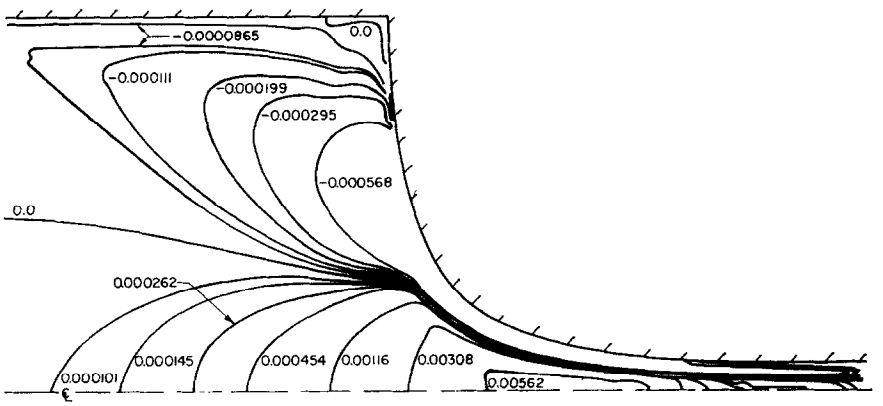

FIG. 11. Normal stress contour lines for a Newtonian fluid.

different from the Newtonian contours, whereas the τ^{22} contours are qualitatively the same. This behavior is to be expected by a cursory comparison of the boundary conditions; the streamwise normal stress reflects the viscoelastic characteristics of the fluid whereas the transverse component exhibits essentially a Newtonian relationship.

APPENDIX A: CONSTRUCTION OF AN ORTHOGONAL CURVILINEAR COORDINATE SYSTEM PARALLEL AND PERPENDICULAR TO THE CONTRACTION BOUNDARY

In order to obtain the proper expressions for the vorticity and stresses in the curvilinear coordinate system it is first necessary to determine the metric tensor for this new system. Let us begin by recalling that the equation of the curved boundary is

$$xy = 0.08, \tag{A1}$$

where the origin of the Cartesian coordinate system is as shown in Fig. 1. Then a family of such curves would be given by

$$\eta = xy. \tag{A2}$$

A family of curves perpendicular to those of Eq. (A2) can be obtained by requiring that the slopes be negative reciprocals of those of the η curves and then integrating; the resulting family of curves is then

$$\phi = (x^2 - y^2)/2. \tag{A3}$$

Therefore in terms of the (ϕ, η) coordinate system, the Cartesian coordinates x and y are given by

$$x = (\phi + (\phi^2 + \eta^2)^{1/2})^{1/2}, \tag{A4}$$

$$y = (-\phi + (\phi^2 + \eta^2)^{1/2})^{1/2}. \tag{A5}$$

Now the metric tensor simply relates the distance to infinitesimal coordinate increments and is defined in the following manner. In a two-dimensional Cartesian system the incremental distance ds can be written as

$$ds^2 = dx^2 + dy^2. \tag{A6}$$

The length ds can be expressed in terms of the (ϕ, η) coordinates by simply transforming contravariantly, then

$$ds^2 = g_{ij}dx^i dx^j = g_{11}d\phi^2 + g_{22}d\eta^2, \tag{A7}$$

where the cross terms are zero in an orthogonal system. Using Eqs. (A4) through (A7) one obtains the nonzero components of the metric tensor for this two-dimensional (ϕ, η) coordinate system

$$g_{11} = g_{22} = (\phi^2 + \eta^2)^{-1/2}/2. \tag{A8}$$

It is also necessary to recall that differentiation in a coordinate system other than a

Cartesian system must take into account the dependence of the transformation on position. Hence one must generalize from partial differentiation to covariant differentiation (and contravariant differentiation). For example, the covariant derivatives of a covariant vector and a contravariant vector are

$$A_{j,k} = \frac{\partial A_j}{\partial x^k} - \Gamma^i_{jk} A_i \,, \tag{A9}$$

$$A^j_{,k} = \frac{\partial A^j}{\partial x^k} + \Gamma^j_{ik} A^i, \tag{A10}$$

where Γ^i_{jk} is the second kind of Christoffel symbol, and is given by

$$\Gamma^i_{jk} = g^{ip} \left\{ \frac{\partial g_{pi}}{\partial x^k} + \frac{\partial g_{pk}}{\partial x^j} + \frac{\partial g_{jk}}{\partial x^p} \right\}. \tag{A11}$$

Using Eqs. (A8) and (A11) one finds the Christoffel symbols in the (ϕ, η) coordinate system as

$$\Gamma^1_{11} = \Gamma^2_{12} = \Gamma^2_{21} = -\phi/2(\phi^2 + \eta^2), \tag{A12}$$

$$\Gamma^2_{22} = \Gamma^1_{12} = \Gamma^1_{21} = -\eta/2(\phi^2 + \eta^2), \tag{A13}$$

$$\Gamma^1_{22} = \phi/2(\phi^2 + \eta^2), \tag{A14}$$

$$\Gamma^2_{11} = \eta/2(\phi^2 + \eta^2). \tag{A15}$$

Finally, it is most convenient to only consider the physical components of the different variables since in this orthogonal system there is no distinction between physical components and the components of mixed tensors. In equation form the physical components of a vector and a tensor can be written as

$$a(i) = g_{ii}^{1/2} a^i = g_{ii}^{-1/2} a_i \qquad \text{(no summation)}, \tag{A16}$$

$$A(ij) = (g_{ii} g_{jj})^{1/2} A^{ij} = (g_{ii} g_{jj})^{-1/2} A_{ij} \qquad \text{(no summation)}, \tag{A17}$$

where $a(i)$ and $A(ij)$ are the physical components of the vector and tensor, respectively.

As can be seen from the above, once the metric tensor has been determined the basic structure of the coordinate system is established and the appropriate differential equations can be determined.

APPENDIX B: Discretizing Errors in the ϕ–η Coordinate System

The accuracy of the finite-difference approximations to the various derivatives in the differential equation is dependent on the grid spacing and higher order derivatives and, in addition, is also dependent on the choice of coordinate system. For example, a

first-order-accurate forward difference approximation of the first derivative in the η-direction would be

$$\psi_\eta = \frac{\psi_{\eta+1,\phi} - \psi_{\eta,\phi}}{\Delta\eta} - \frac{\Delta\eta}{2}\psi_{\eta\eta} + \text{higher-order terms}, \tag{B1}$$

where $\psi_{\eta+1,\phi}$ and $\psi_{\eta,\phi}$ are discretized grid locations of the variable ψ in the $\phi - \eta$ plane and $\Delta\eta$ is the grid spacing in that system. It would then appear that as $\Delta\eta$ goes to zero the difference approximation more closely approximates the derivative; however, closer examination reveals that this is not the case at the origin of the coordinate system. Consider the error term in Eq. (B1). The second derivative $\psi_{\eta\eta}$ can be expressed in terms of x and y derivatives of the Cartesian base system by

$$\psi_{\eta\eta} = \left(\frac{\partial x}{\partial \eta}\right)^2 \psi_{xx} + 2\left(\frac{\partial x}{\partial \eta}\right)\left(\frac{\partial y}{\partial \eta}\right)\psi_{xy} + \left(\frac{\partial y}{\partial \eta}\right)^2 \psi_{yy} + \frac{\partial^2 x}{\partial \eta^2}\psi_x + \frac{\partial^2 y}{\partial \eta^2}\psi_y, \tag{B2}$$

where

$$\frac{\partial x}{\partial \eta} = \frac{\eta}{2(\phi^2+\eta^2)^{1/2}(\phi^2+(\phi^2+\eta^2)^{1/2})^{1/2}},$$

$$\frac{\partial y}{\partial \eta} = \frac{\eta}{2(\phi^2+\eta^2)^{1/2}(-\phi+(\phi^2+\eta^2)^{1/2})^{1/2}},$$

$$\frac{\partial^2 x}{\partial \eta^2} = \frac{1}{2(\phi^2+\eta^2)^{1/2}(\phi+(\phi^2+\eta^2)^{1/2})^{1/2}}\left\{1 - \frac{\eta^2}{\phi^2+\eta^2} - \frac{\eta^2}{(\phi^2+\eta^2)^{3/2}(\phi+(\phi^2+\eta^2)^{1/2})}\right\},$$

$$\frac{\partial^2 y}{\partial \eta^2} = \frac{1}{2(\phi^2+\eta^2)^{1/2}(-\phi+(\phi^2+\eta^2)^{1/2})^{1/2}}\left\{1 - \frac{\eta^2}{\phi^2+\eta^2} - \frac{\eta^2}{(\phi^2+\eta^2)^{3/2}(-\phi+(\phi^2+\eta^2)^{1/2})}\right\}.$$

It is clear from the above equations that a singularity exists at the point (0, 0) in the ϕ–η plane (which is also the origin of the Cartesian system) and, in addition, this same problem arises when the second derivative with respect to ϕ is analyzed. From the above calculations it also appears that higher-order derivatives would retain this singular character, thus making higher-order difference schemes just as inaccurate. This problem is simply a consequence of the fact that the metric is singular at the origin and that variables calculated near the origin in the curvilinear system are not properly mapped into the Cartesian system. Numerical tests indicated, however, that this problem is isolated very close to the origin and that specification of the boundary conditions along the curved boundary in the ϕ–η system was not in error.

ACKNOWLEDGMENTS

This work was supported in part by the U.S. Naval Ordinance Systems Command, through the Fluids Engineering Unit of the Applied Research Laboratory, and in part by the U.S. Office of Naval Research, Fluid Dynamics Branch: It formed part of the Ph.D. thesis of Thomas B. Gatski [1].

REFERENCES

1. T. B. GATSKI, "The Numerical Solution of the Steady Flow of Newtonian and Non-Newtonian Fluids through a Contraction," Ph.D. Thesis, Pennsylvania State University, 1976.
2. H. GIESEKUS, *Rheol. Acta.* **2** (1962), 50.
3. J. L. LUMLEY, *Phys. Fluids* **14** (1971), 2282.
4. J. G. OLDROYD, *Proc. Roy. Soc. Ser. A* **200** (1950), 523.
5. T. B. GATSKI, *J. Computational Phys.* **19** (1975), 376.
6. P. TOWNSEND, *Rheol. Acta* **12** (1973), 13.
7. N. D. WATERS AND M. J. KING, *J. Phys. D* **4** (1971), 204.
8. A. K. RUNCHAL AND M. WOLFSHTEIN, *J. Mech. Eng. Sci.* **11** (1969), 445.
9. F. B. HILDEBRAND, "Introduction to Numerical Analysis," McGraw–Hill, New York, 1956.
10. D. GREENSPAN, *J. Eng. Math.* **3** (1969), 21.
11. A. J. FABULA, "An Experimental Study of Grid Turbulence in Dilute High-Polymer Solutions," Ph.D. Thesis, Pennsylvania State University, 1966.
12. P. J. ROACHE, "Computational Fluid Dynamics," Hermosa, Albuquerque, N. Mex. 1972.
13. G. K. BATCHELOR, "An Introduction to Fluid Dynamics," Cambridge Univ. Press, London, 1967.
14. J. L. LUMLEY, *Symposia Mathematica* **9** (1972), 315.